

Simulations of Cell Behavior on Substrates of Variegated Stiffness and Architecture

Amit Pathak, Vikram S. Deshpande, A. G. Evans, Robert M. McMeeking

Abstract Several experimental studies have shown that cells adhered to stiffer substrates exert higher traction forces and simultaneously form more prominent focal adhesions and stress fibers. We employ a bio-chemo-mechanical model implemented in a finite element framework to simulate cell response on substrates of variegated stiffness and architecture. We perform simulations to generate stress fiber and focal adhesion distributions, and predict the values of forces generated by cells adhered on flat gels and on beds of micro-posts of variegated stiffness. We also demonstrate that our predictions agree well with the available experimental measurements obtained with the same cell-substrate setting. For a given, calibrated set of model parameters, our traction force predictions for cells adhered to post-beds of varying stiffness match with measurements from Saez et al. (2005). Actin and focal adhesion distributions obtained from our simulations agree well with the patterns observed in the results of various visualization experiments available in the literature. Taken together, these findings suggest that our model captures well the intricate coupling mechanisms arising from cell-substrate interaction and intracellular machinery.

Amit Pathak
Department of Mechanical Engineering, University of California, Santa Barbara, CA 93106, USA
e-mail: amitp@berkeley.edu

Vikram S. Deshpande
Engineering Department, Trumpington Street, Cambridge University, Cambridge CB2 1PZ, UK
e-mail: vsd@eng.cam.ac.uk

Robert M. McMeeking
Department of Mechanical Engineering, University of California, Santa Barbara, CA 93106, USA
Materials Department, University of California, Santa Barbara, CA 93106, USA
School of Engineering, Aberdeen University, King's College, Aberdeen AB24 3UE, UK
INM - Leibniz Institute for New Materials, Campus D2 2, 66123 Saarbrücken, Germany
e-mail: rmcm@engineering.ucsb.edu

1 Introduction

Living cells interact with their environments over a wide range of stiffness, from soft skin through stiffer muscle to harder bone substrates. In such cellular interactions, adhesion of cells to substrates or to an extra-cellular matrix (ECM) is a critical feature in many cellular functions, ranging from migration and proliferation to apoptosis (Boudreau and Bissell, 1998; Schwartz and Ginsberg, 2002). Experimental studies have now shown that the mechanical compliance of the ECM or the substrate influences cell viability, differentiation and motility (Lo et al., 2000; Discher et al., 2005; Yeung et al., 2005). It is now widely accepted that cells exert a higher force, form larger focal adhesions and develop thicker stress fibers on stiffer substrates (Saez et al., 2005; Yeung et al., 2005). The relationship between stiffness and intracellular machinery regulates many important functions such as non-viral gene delivery (Kong et al., 2005) and growth of cancer cells (Paszek et al., 2005). Evidence suggests that increased rigidity may trigger malignant transformation (Paszek et al., 2005), attributable to increased cytoskeletal tension, integrin clustering and focal adhesion formation.

The experimental studies by Saez et al. (2005) and Yeung et al. (2005) clearly demonstrate a direct dependence of cell behavior on substrate stiffness. In these studies, cellular activity, measured in terms of the average force exerted by the cell on the substrate, the size of focal adhesions, and the concentration of stress fibers, rose to greater levels on stiffer substrates. In addition, the experimental studies of Tan et al. (2003) and Chen et al. (2003) provide further data regarding the shape and size of cell-substrate adhesions and the scaling of forces relative to the spread area of the cell.

A recently developed bio-chemo-mechanical model by Deshpande et al. (2006, 2007, 2008) characterizes the dynamically contractile stress fiber machinery made of actin-myosin filaments, giving rise to intracellular force generation, as well as focal adhesion assembly, the latter based on thermodynamic equilibrium between integrins in their low and high affinity states. This model has been successfully employed in simulations of experiments, including cell adhesion on V, T, Y and U-shaped patterned substrates (Pathak et al., 2008), and the formation of stress fibers upon cyclic stretching (Wei et al., 2008). We utilize a similar approach to simulate cell behavior on flat gel substrates, and on post-beds of variegated stiffness. While post-beds offer direct and readily quantifiable insights into the shapes and sizes of adhesions and the forces applied by a contractile cell, a flat substrate is relevant due to its presence in living organisms and its use for in vitro studies. Here, we present simulations for both flat substrates and post-beds, and predict trends in focal adhesion distribution, tractions and stress fiber distribution common to both types of substrate architecture.

2 A Bio-Chemo-Mechanical Model for the Cell

We envisage a well-spread, approximately two-dimensional cell, thickness b , lying on a substrate in the x_1 - x_2 plane. The cell model comprises two major elements: (i) a constitutive model for the formation of stress fibers, their contractility and their spontaneous attachment to cell adhesion complexes; (ii) a cell adhesion model causing the cell to adhere to a substrate. In (i), following an activation signal, the model predicts the development of contractile, actin-myosin stress fibers by polymerization, subject to their spontaneous connection to trans-membrane adhesions, and consistent with traction or displacement conditions imposed by these adhesions at the interface between the cell and its substrate. The outputs of this feature of the model are the spatial (position x_i) and temporal (time t) distributions of the stress fiber concentration, $\eta(x_i, \phi, t)$ and the Cauchy stresses $\Sigma_{ij}(x_i, t)$ generated by the resulting stress fiber contractility, where ϕ is the angle of orientation of a given family of stress fibers. In (ii), the stresses generated by the stress fiber model apply tractions to the focal adhesions to which the stress fibers are attached, and, thereby, control the spatial and temporal development of such adhesions, as parameterized through the high affinity integrin concentration on the cell membrane at the interface with the substrate. Such high affinity integrins are the trans-membrane proteins, bound to stress fibers in the cell and substrate ligands outside it, that are the most important molecules forming the adhesion between the cell cytoskeleton and the substrate to which it is attached. Note that there are two main sources of mechano-sensitivity in the model as described below; tension in the stress fibers tends to inhibit their depolymerization, and tractions transmitted through adhesion complexes stabilizes them, encouraging formation of trans-membrane integrins bound to ligands on the substrate.

The mechanical equilibrium equations for the cell are written as

$$b \left(\frac{\partial \Sigma_{11}}{\partial x_1} + \frac{\partial \Sigma_{12}}{\partial x_2} \right) = \xi_H F_1, \quad b \left(\frac{\partial \Sigma_{12}}{\partial x_1} + \frac{\partial \Sigma_{22}}{\partial x_2} \right) = \xi_H F_2, \quad (1)$$

where $\xi_H(x_i, t)$, the concentration of high affinity, bound integrins, is their number per unit current area of the cell membrane, and F_i is the force per high affinity integrin applied by the cell to the substrate.

2.1 Stress Fiber Formation and Contractility

Stress fiber formation is initiated by a nervous impulse or a biochemical or mechanical perturbation that triggers a signaling cascade within the cell. We model this signal, C (which may be thought of as the concentration of Ca^{2+}) as a sudden rise to unity followed by an exponential decay, given by

$$C = \exp(-t_i/\theta), \quad (2)$$

where θ is the decay constant and t_i is the time after the onset of the most recent activation signal. We treat the signal as uniform throughout the cell, on the basis that diffusion of the signaling ions and proteins in the cytosol is fast enough to be non-rate limiting, as determined by Pathak et al. (2011).

The formation of stress fibers is parameterized by an activation level, designated η ($0 \leq \eta \leq 1$), defined as the ratio of the concentration of the polymerized actin and phosphorylated myosin within a stress fiber bundle to the maximum concentrations permitted by the bio-chemistry. The evolution of the stress fibers at an angle ϕ to the x_1 axis is characterized by a first-order kinetic equation

$$\dot{\eta}(\phi) = [1 - \eta(\phi)] \frac{C\bar{k}_f}{\theta} - \left(1 - \frac{\sigma(\phi)}{\sigma_0(\phi)}\right) \eta(\phi) \frac{\bar{k}_b}{\theta}, \quad (3)$$

where the overdot denotes time-differentiation at a fixed material point in the cell. In this formula, $\sigma(\phi)$ is the tension in the fiber bundle at orientation ϕ , while $\sigma_0(\phi) = \eta \sigma_{\max}$ is the corresponding isometric stress at activation level η , with σ_{\max} being the isometric stress at full activation ($\eta = 1$). The dimensionless constants \bar{k}_f and \bar{k}_b govern the rates of stress fiber formation and dissociation, respectively. Note that mechano-sensitivity is present in the depolymerization term in (1), since a tensile stress σ will reduce the rate of dissociation of stress fibers; furthermore, a stress σ equal to σ_0 eliminates stress fiber depolymerization completely.

The stress σ in stress fibers is related to the fiber contraction/extension rate $\dot{\epsilon}$ (positive during extension) by the cross-bridge cycling between the actin and myosin filaments. The simplified (but adequate) version of the Hill-like equation employed to model these dynamics is specified as

$$\frac{\sigma}{\sigma_0} = \begin{cases} 0 & \frac{\dot{\epsilon}}{\dot{\epsilon}_0} < -\frac{\eta}{\bar{k}_v}, \\ 1 + \frac{\bar{k}_v}{\eta} \left(\frac{\dot{\epsilon}}{\dot{\epsilon}_0} \right) & -\frac{\eta}{\bar{k}_v} \leq \frac{\dot{\epsilon}}{\dot{\epsilon}_0} \leq 0, \\ 1 & \frac{\dot{\epsilon}}{\dot{\epsilon}_0} > 0, \end{cases} \quad (4)$$

where the rate sensitivity coefficient \bar{k}_v is the fractional reduction in fiber stress upon increasing the shortening rate by $\dot{\epsilon}$. A 2-d constitutive description for the stress fiber assembly uses the axial fiber strain rate $\dot{\epsilon}$ at angle ϕ related to the strain rate $\dot{\epsilon}_{ij}$ by

$$\dot{\epsilon} = \dot{\epsilon}_{11} \cos^2 \phi + \dot{\epsilon}_{22} \sin^2 \phi + \dot{\epsilon}_{12} \sin 2\phi. \quad (5)$$

The average stress generated by the fibers follows from a homogenization analysis as

$$\begin{pmatrix} S_{11} & S_{12} \\ S_{21} & S_{22} \end{pmatrix} = \frac{1}{\pi} \int_{-\pi/2}^{\pi/2} \begin{pmatrix} \sigma(\theta) \cos^2 \phi & \frac{\sigma(\theta)}{2} \sin 2\phi \\ \frac{\sigma(\theta)}{2} \sin 2\phi & \sigma(\theta) \sin^2 \phi \end{pmatrix} d\phi. \quad (6)$$

The constitutive description for the cell is completed by including contributions from passive elasticity, attributed to intermediate filaments of the cytoskeleton attached to the nuclear and plasma membranes. These act in parallel with the active elements, whereupon additive decomposition gives the total stress:

$$\Sigma_{ij} = S_{ij} + \left[\frac{E_c \nu_c}{(1 - 2\nu_c)(1 + \nu_c)} \varepsilon_{kk} \delta_{ij} + \frac{E_c}{(1 + \nu_c)} \varepsilon_{ij} \right], \quad (7)$$

where δ_{ij} is the Kronecker delta and (for a linear response) E_c is Young's modulus for the cell and ν_c the Poisson ratio. The above equations are valid in a small or infinitesimal deformation setting; readers are referred to Deshpande et al. (2006, 2007) for the finite strain and three-dimensional generalization.

2.2 Focal Adhesion Model

A viable model for the formation and growth of focal adhesions must account for the interaction between adhesions and cell contractility. The Deshpande et al. (2008) model relies on the existence of two conformational states for the integrins: low and high affinity. Only the high affinity integrins interact with ligand molecules on the substrate to form adhesions. The low affinity integrins remain unbound, and mobile on the membrane. The chemical potential of the low affinity integrins at concentration L is dependent on their internal energy and configurational entropy as (Gaskell, 1973)

$$\chi_L = \mu_L + kT \ln(\xi_L / \xi_R), \quad (8)$$

where μ_L is their reference chemical potential, ξ_R is a reference concentration, k is the Boltzmann constant and T the absolute temperature.

For geometrical reasons, the 'straight' architecture of the high affinity integrins permits the interaction of its receptor with ligand molecules on a substrate. Thus, the high affinity integrins have additional contributions to their chemical potential, involving the energy stored due to the stretching of the integrin-ligand complexes and a term related to the mechanical work done by the stress fibers. The ensuing potential is

$$\chi_H = \mu_H + kT \ln(\xi_H / \xi_R) + \Phi(\Delta_i) - F_i \Delta_i, \quad (9)$$

where μ_H is the reference chemical potential for high affinity integrins and $\Phi(\Delta_i)$ is the stretch energy stored in the integrin-ligand complex. The 'straight,' high affinity state of the integrins is less stable than the 'bent' or low affinity state (McCleverty and Liddington, 2003) so that the high affinity state has the higher reference chemical potential ($\mu_H > \mu_L$). The $-F_i \Delta_i$ term in eq. (9) is the mechanical work representing the change in free energy due to the stretch Δ_i of the integrin-ligand complex acted upon by the force F_i . In molecular terms this implies that the stretch

of the ligand-integrin complex can stabilize the adhesion by lowering the free energy ξ_H of bound integrins. The force F_i is related to the stretch Δ_i and the stored energy Φ via the relation

$$F_i = \partial\Phi/\partial\Delta_i. \quad (10)$$

The work term $-F_i\Delta_i$ term in eq. (9) has been identified previously by Shemesh et al. (2005) as an important constituent of the thermodynamic state of focal adhesions.

The kinetics governing the diffusion of low affinity integrins in the cell membrane is typically fast compared to all other time-scales involved (Deshpande et al., 2008; Pathak et al., 2011). Consequently, we neglect the diffusion of the low affinity integrins and the kinetics between their low and high affinity states at any location on the plasma membrane. These simplifying assumptions imply that the concentrations are given by thermodynamic equilibrium between the low and high affinity binders, i.e. by

$$\chi_H = \chi_L, \quad (11)$$

which specifies that the integrin concentrations are related to the force F_i via

$$\xi_H = \frac{\xi_0}{\exp\left(\frac{\mu_H - \mu_L + \Phi - F_i\Delta_i}{kT}\right) + 1}, \quad (12)$$

$$\xi_L = \frac{\xi_0}{\exp\left(-\frac{\mu_H - \mu_L + \Phi - F_i\Delta_i}{kT}\right) + 1}, \quad (13)$$

respectively, where $\xi_0 = \xi_H + \xi_L$ is the fixed, total concentration of integrins. It is evident that with decreasing $\Phi - F_i\Delta_i$ (which typically occurs when the tensile force F_i increases), the concentration ξ_H of the high affinity integrins increases due to the conversion of the low affinity integrins to their high affinity state.

To complete the thermodynamic representation it remains to specify the form of the energy $\Phi(\Delta_i)$ and the associated force F_i in the integrin-ligand complex. Rather than employing a complex interaction, such as the Lennard-Jones (1931) potential, we utilize the simplest functional form. This is a piecewise quadratic potential expressed as (Deshpande et al., 2008)

$$\Phi = \begin{cases} (1/2)\kappa_s\Delta_e^2 & \Delta_e \leq \Delta_n, \\ -\kappa_s\Delta_n^2 + 2\kappa_s\Delta_n\Delta_e - (1/2)\kappa_s\Delta_e^2 & \Delta_n < \Delta_e \leq 2\Delta_n, \\ \kappa_s\Delta_n^2 & \Delta_e > 2\Delta_n, \end{cases} \quad (14)$$

where $\gamma \equiv \Phi(\Delta_i \rightarrow \infty) = \kappa_s\Delta_n^2$ is the surface energy due to high affinity integrins, the effective stretch $\Delta_e^2 = \Delta_1^2 + \Delta_2^2$, and κ_s is the stiffness of the integrin-ligand complex. The maximum force $\kappa_s\Delta_n$ occurs at a stretch $\Delta_e = \Delta_n$. We relate the evolution of

the stretch Δ_i to the displacement u_i of the material point on the cell membrane in contact with the ligand patch on the substrate as (Deshpande et al., 2008)

$$\dot{\Delta}_i = \begin{cases} \dot{u}_i, & \Delta_e \leq \Delta_n \quad \text{or} \quad \left(\frac{\partial \Phi}{\partial \Delta_e} \dot{\Delta}_e < 0 \right), \\ 0, & \text{otherwise,} \end{cases} \quad (15)$$

where we assume a rigid substrate (see Deshpande et al., 2008, for the generalization to a deformable substrate as used here).

Those integrins not in contact with the ligand patch are assumed to be isolated. Namely, they are unable to interact with any ligand molecules. Accordingly, we assume that these integrins are unbonded with $\Delta_i \rightarrow \infty$ such that the interaction force $F_i = 0$ and energy $\Phi = \gamma$. Their concentrations are then given by eqs. (12) and (13) with such values inserted.

2.3 Finite Element Framework

The contractility model for the cell behavior is implemented in the ABAQUS finite element model using a user UMAT subroutine that calculates the material response of the cell in terms of actin polymerization and force generation. The interfacial behavior between the cell and a substrate is implemented via the UINTER subroutine, responsible for force equilibrium of the entire cell-substrate system and focal adhesion development at the cell-substrate interface. Parameters for the contractility and focal adhesion models are calibrated using the cell-on-posts simulation presented in Section 4. Based on this calibration study the following reference material parameters are chosen, with $T = 310$ K. The modulus $E_c = 0.9$ kPa and the Poisson ratio $\nu_c = 0.3$. The reaction rate constants are $\bar{k}_f = 10$, $\bar{k}_b = 1$, $\bar{k}_v = 6$ with $\dot{\epsilon}_0 = 3.0 \times 10^{-3} \text{ s}^{-1}$, while the maximum tension exerted by the stress fibers is $\sigma_{\max} = 15$ kPa. For the focal adhesion model, the total concentration ξ_o is taken to be $5000 \text{ integrins}/\mu\text{m}^2$, and the difference in the reference chemical potentials is taken as $\mu_H - \mu_L = 5 \text{ kT}$. We choose an integrin-ligand complex stiffness $\kappa_s = 0.015 \text{ nNm}^{-1}$, and the stretch at maximum force $\Delta_n = 130 \text{ nm}$, giving a bond strength $\sim 2 \text{ pN}$. Throughout the simulations presented in this article these parameters are kept constant and only the substrate properties are varied.

2.4 Correlation Between Model Parameters and Experimental Results

Focal adhesions are imaged in experiments by staining for the protein vinculin, which directly correlates to the concentration ξ_H of the high affinity integrins. The corresponding characterizing parameter for the stress fiber distributions is not cho-

sen so straightforwardly. Most techniques only image the dominant stress fibers. The very fine mesh-work of actin filaments is not visible when standard epifluorescence or confocal microscopes are used. Thus, to correlate the observations with the predictions we define a circular variance $\Gamma = 1 - (\bar{\eta}/\eta_{\max})$, used by Pathak et al. (2008), that provides an estimate of how tightly the stress fibers are clustered around a particular orientation. Here η_{\max} is the maximum polymerization level, which occurs at orientation ϕ_s , while $\bar{\eta}$ is an average value defined as $\bar{\eta} \equiv 1/\pi \int_{-\pi/2}^{\pi/2} \eta d\phi$. The value of Γ varies from 0 to 1, corresponding to perfectly uniform and totally aligned distributions, respectively.

3 Modeling Cell Behavior on Flat Substrates of Variegated Stiffness

We first investigate the cell-substrate interaction where a single cell is adhered to a flat surface. In our simulations, we utilize isotropic material properties for the flat substrate on which the cell attaches and forms focal adhesions. The stiffness of the substrate is prescribed by its Young's modulus.

3.1 Finite Element Implementation

The cell behavior is investigated in a finite strain setting (i.e. the effects of geometry changes on the momentum balance and constitutive behavior through material rotations are taken into account). We implement a 3-d model of the gel using 8-noded linear brick elements, and a cell composed of membrane elements of unit thickness. We choose a circular cross-section for both the gel and the cell to obviate any geometrical irregularities in the simulations. The diameter of the cell is $34 \mu\text{m}$. The gel diameter and thickness are taken to be approximately $350 \mu\text{m}$ to emulate the experiments where a cell is laid on a relatively thick gel substrate. Simulations based on the chosen geometry show that the reaction forces in the gel substrate are negligible away from the cell; thus, the chosen setup behaves like a cell lying on an infinitely thick gel substrate.

In each simulation, we start with a quiescent, stress free cell, having no stress fibers and a negligible quantity of adhesions (there exist a few that keep the cell located in place on the gel, consistent with eqs. (12) and (13)). To commence the simulation, we turn on the signal in eq. (2) at time $t = 0$, which has the effect of causing the formation of stress fibers and focal adhesions. Progressive polymerization and depolymerization of stress fibers, the growth of focal adhesions, and the generation of contractile stress take place within the cell. This process is continued in the simulation until a steady state is reached, with a stable configuration of stress fibers, mature focal adhesions, and a constant stress at any given location in the cell.

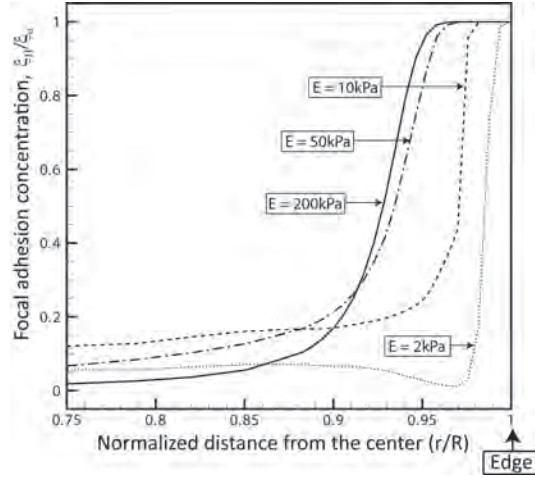


Fig. 1 Steady state focal adhesion distributions for a circular cell adhered to a flat gel substrate of Young's moduli varying from 2 to 200 kPa, where R is the radius of the cell.

3.2 Simulation Results

We vary the stiffness of the gel, characterized by its Young's Modulus E from 2 to 200 kPa and record the cell behavior. We calculate the focal adhesion distribution as the normalized concentration ξ_H/ξ_o of the high affinity integrins at each node, i.e. a focal adhesion is taken as a region where ξ_H/ξ_o is high. The results are presented in Fig. 1, where axial symmetry permits the distributions to be plotted versus radial position. We find that on a relatively soft gel of $E = 2$ kPa, the cell does not develop prominent focal adhesions. However, on the stiffer gels focal adhesions develop to a much higher degree with their highest concentration at the periphery. The plot in Fig. 1 demonstrates that cells form larger focal adhesions on stiffer substrates, in qualitative agreement with many experimental studies, including that by Saez et al. (2005). To further elucidate this point we plot the cell total focal adhesion fraction ξ_T in steady state versus the stiffness of the substrate E in Fig. 2(a). Here, the cell total focal adhesion fraction ξ_T is calculated by integrating the concentration ξ_H over the entire cell area and dividing the result by the total number of integrins $\xi_o A$ on the cell membrane, where A is the area of the cell. As a result, ξ_T is the fraction of all integrins on the cell membrane that are in the high affinity state, and thus in focal adhesions. As expected, ξ_T increases for stiffer substrates, but reaches an asymptote at approximately $E = 50$ kPa. Any further rise in stiffness beyond this level does not change the overall focal adhesion distribution, a trend also apparent in Fig. 1.

We compute the magnitude of the cell traction applied to the substrate as $\xi_H(F_1^2 + F_2^2)^{1/2}$, and integrate this over the interface between the cell membrane and the gel to obtain a total force magnitude F_T applied by the cell to the substrate (we note here to avoid confusion that the total force vector applied by the cell to the gel is

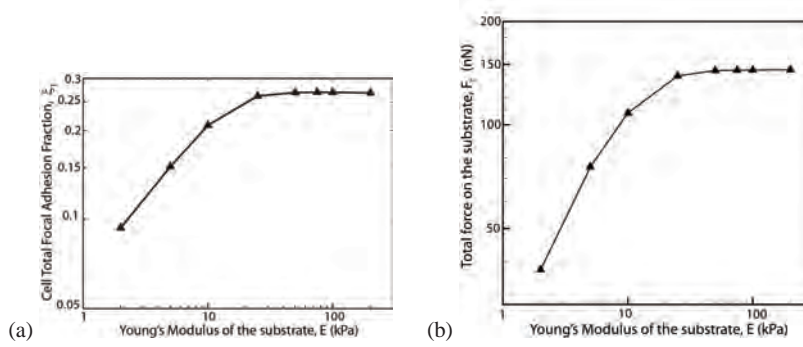


Fig. 2 (a) Cell total focal adhesion fraction F_T and (b) total force F_T exerted by a cell adhered to a flat gel substrate in steady state, where Young's modulus E of the gel is varied from 2 to 200 kPa.

zero, but view the parameter F_T as a useful gauge of the intensity of force generation associated with the contractile machinery of the cell). We find that the total force F_T increases as the substrate stiffness E is increased, as shown in Fig. 2(b), but reaches an asymptote beyond $E = 50$ kPa. In addition, we also establish a linear correlation between focal adhesion assembly and force generation by plotting F_T versus ξ_T (not shown).

We note that the total force F_T applied by the cell to the gel is also an indicator of the degree of stress fiber development. Although we do not plot the results, we can confirm that in our simulations, cells on stiffer gels have higher average concentrations of stress fibers compared to cells on more compliant gels. Consistent with the trends in Figs. 1 and 2, the average concentration of stress fibers in a cell reaches an asymptote at a gel modulus of approximately 50 kPa.

4 Models of Cell Behavior on Micro-Posts

The distribution of traction forces exerted by a cell on its adhered substrate has been measured by seeding cells on a bed of micro-posts and determining the independent deflections of the posts (Tan et al., 2003; Saez et al., 2005). The isolated islands of cell-substrate interaction on post tops allow discrete measurement of traction forces, and the size and shape of focal adhesions. In the experiments of Saez et al. (2005), the stiffness of the posts is varied and the average force per post F_{avg} exerted by the cell is recorded. This quantitative study demonstrates that the average force per post increases as the post stiffness is increased regardless of post-bed geometry or cell area. We use these measurements to test our model, and, as noted above, to calibrate it.

On top of the posts, the cell forms adhesions; the studies by Tan et al. (2003) and Chen et al. (2003) find that (a) focal adhesions, measured by vinculin staining, on top of posts near the edge of the cell are the largest, (b) posts interior to the cell have

negligible focal adhesions, and (c) the focal adhesion distribution forms a horseshoe shape around the top perimeter of the posts. In addition, Tan et al. (2003) found that F_{avg} increases with the size of a cell, a behavior that can be rationalized by recognition that a larger cell pulls on more posts, so experiencing a stiffer environment.

4.1 Finite Element Setup for Cells on Posts

We use square cells having various areas, and model the posts as rigid circular discs of radius $a = 1 \mu\text{m}$ constrained to move in the x_1 - x_2 plane. The displacement d_i of the discs is constrained by a spring of stiffness k (SPRING1 option in ABAQUS) such that the force P_i applied by the cell is $P_i = kd_i$. We implement the adhesion between the cell and the disc surfaces by employing the user-defined interface (UINTER) option in ABAQUS, as before. Adhesions are allowed to form only where the cell is in contact with the discs. We keep the post area fraction, defined as the ratio of total surface area of the post-tops in contact with the cell to the total cell area, at approximately 25% to match the characteristics of the post-bed used by Saez et al. (2005).

As in the simulations for cells on flat gel substrates, we commence with stress free, quiescent cells having neither stress fibers nor significant adhesions, and initiate the computation with a single signal. After transient behavior, a steady state sets in, with a constant stress state and stress fiber concentration and distribution at any point in the cell, a constant focal adhesion concentration at any point on the top of a post, and a constant deflection of the top of each post.

4.2 Simulation Results and Discussion

We first address simulations for a square cell of edge length $L = 30 \mu\text{m}$ that covers an 8×8 post array.

4.2.1 Focal Adhesion and Stress Fiber Distribution

We consider first highly compliant posts having a spring constant $k = 2 \text{ nN}/\mu\text{m}$. As shown in Fig. 3(a), a plot of the concentration of high affinity integrins in steady state, focal adhesions form a circular ring on each post with little polarization, and with relatively low densities of high affinity integrins. We interpret this to mean that the size of focal adhesions on these posts is small, even though they completely surround the tops of the posts. We implicate the very low stiffness of the posts used in this case for this behavior. Such compliant posts offer little resistance to stress fiber contractility, obviating the generation of tension in the stress fibers and allowing much depolymerization. The resulting lack of intracellular machinery in

steady state is evident in the low stress fiber concentrations observed for this case, and in the lack of curvature along the edge of the cell, as depicted in Fig. 3(a). In Fig. 4(a) we show the distribution of stress fibers for this case, characterized by the parameter Γ . A modest degree of alignment of stress fibers is evident in this figure, but the significance of this is reduced by the fact that the stress fiber concentration at each point in the cell is relatively low. We note that each post top is interacting individually with the cell region that surrounds it, and there is little mechanical communication among posts and between different locations in the cell. This feature explains the lack of polarization of the focal adhesions into a horseshoe shape on the post tops. The shape of the focal adhesion rings on the post tops and a lack of overall contractility in these simulations matches the experimental observations of Chen et al. (2003), where focal adhesions form uniformly in a ring shape on a circular substrate upon pharmacological inhibition of actomyosin contractility.

We next consider posts having a stiffness $k = 10 \text{ nN}/\mu\text{m}$. Such posts are sufficiently stiff that the resistance they offer to cell contractility inhibits the rate of depolymerization of stress fibers, and allows the generation of higher contractile stress. As a result, the tractions applied to high affinity integrins are high enough to stabilize them, and significant focal adhesion form, as shown in Fig. 3(b). Note that the posts in the interior of the cell do not have significant focal adhesions, while posts near the cell perimeter have larger focal adhesions in a horseshoe shape with their open side directed towards the cell center, as in the experimental results of Chen et al. (2003), shown in Fig. 3(e). In these experiments, chemically boosted intracellular contractile activity causes significant stress in the cell, responsible for higher focal adhesion densities near the cell periphery and the polarized horseshoe shape on individual posts. The fact that there is a significant density of contractile stress fibers is reflected in the curvature of the cell edge visible in Fig. 3(b). The heterogeneous nature of the cell response is more pronounced in this case than for the more compliant posts, evidenced by the degree of alignment of stress fibers shown in Fig. 4(b). The distribution of stress fiber orientations is almost uniform at the center of the cell, whereas they are highly aligned along the cell edge. This and other features visible in Figs. 3(b) and 4(b) indicate that posts near the cell perimeter are interacting with other perimeter posts to a significant degree via the stress fibers, and are interacting with the cell as a whole. Furthermore, the stress at the center of the cell is relatively high, only falling rapidly near the cell edges in a shear lag phenomenon. The stress gradient there is what gives rise to the horseshoe shape of the focal adhesions on posts near the cell perimeter, as the force applied by the cell to an individual post has a net resultant acting towards the open side of the horseshoe. A high, almost uniform stress at the cell center explains the relative lack of focal adhesions on posts near the cell center (Fig. 3(b)), as the absence of a stress gradient means that little force is being applied to the post tops in that area.

Next, we consider the simulations for posts with even higher stiffness, $k = 10 \text{ nN}/\mu\text{m}$, with the focal adhesion distribution shown in Fig. 3(c). In this case, spatial gradients of stress near the cell perimeter are steeper than for more compliant posts. As a result, the concentration of focal adhesions on posts near the cell periphery is even higher than for the more compliant posts, and the horseshoe shape

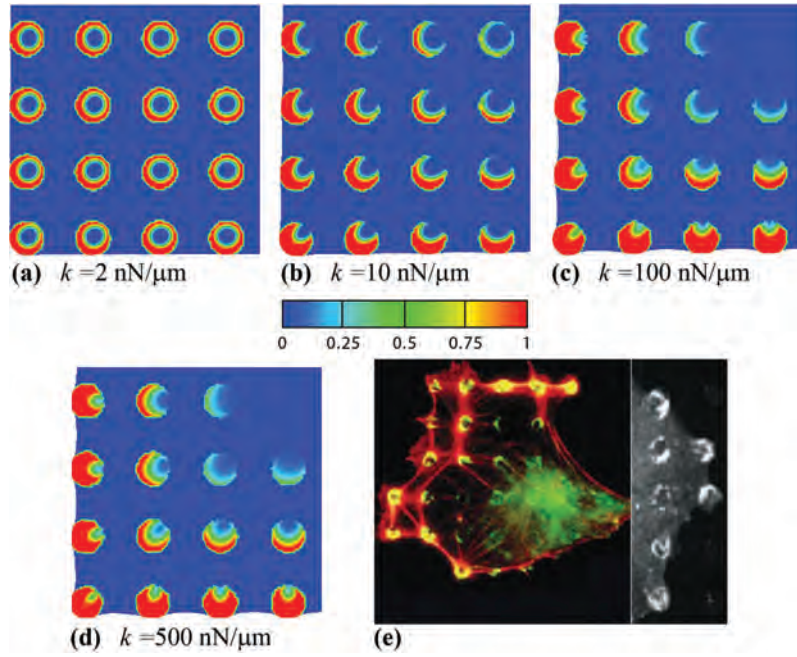


Fig. 3 Contour plots of focal adhesion concentration, defined by the quantity ξ_H/ξ_o , for a cell adhered in steady state to a post-bed with post stiffness (a) $k = 2 \text{ nN}/\mu\text{m}$, (b) $k = 10 \text{ nN}/\mu\text{m}$, (c) $k = 100 \text{ nN}/\mu\text{m}$, and (d) $k = 500 \text{ nN}/\mu\text{m}$. Only quarter segments of the square cells are shown. (e) Focal adhesion distributions on post tops from the experiments of Chen et al. (2003) and Tan et al. (2003).

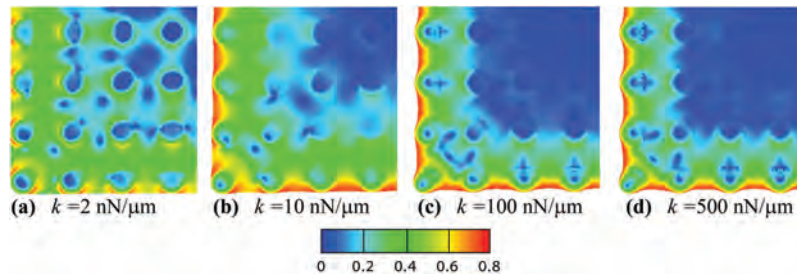


Fig. 4 Contour plots of the distribution of stress fiber orientations, characterized by the quantity Γ , for a cell in steady state adhered to a post-bed with post stiffness (a) $k = 2 \text{ nN}/\mu\text{m}$, (b) $k = 10 \text{ nN}/\mu\text{m}$, (c) $k = 100 \text{ nN}/\mu\text{m}$, and (d) $k = 500 \text{ nN}/\mu\text{m}$. Only quarter segments of the square cells are shown.

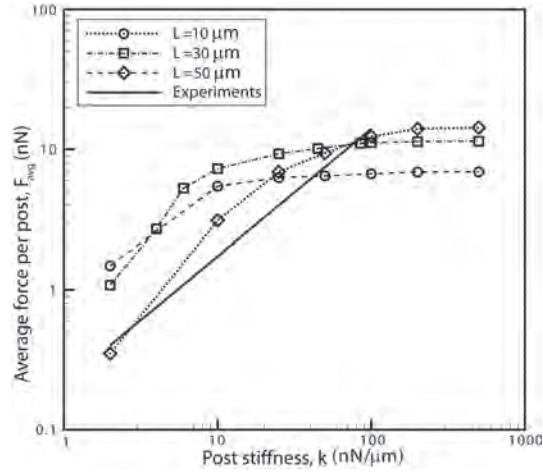


Fig. 5 Average force per post F_{avg} exerted by a square cell in steady state vs. post stiffness k for cells of edge lengths L .

of the focal adhesion distribution on these posts becomes more distinct. Note also that the concentration of focal adhesions on posts near the center of the cell is lower than for the more compliant posts, indicating a more uniform stress there when the posts are stiff. The contractile stress and the concentration of stress fibers in the cell are greater than for the more compliant posts, as can be deduced from the higher curvature of the cell edge visible in Fig. 3(c). The heterogeneous nature of the response of the cell is apparent in the degree of alignment of the stress fibers, shown in Fig. 4(c), with an almost uniform distribution of orientations in a large patch at the center of the cell, and a high degree of alignment around the cell perimeter. This reflects the larger gradient of stress and stress fiber concentration near the cell edge in this case.

We find that increasing the post stiffness further to $k = 500 \text{ nN}/\mu\text{m}$ does not cause appreciable changes in the focal adhesion and stress fiber distributions, as shown in Figs. 3(d) and 4(d), respectively. Thus, the cellular response reaches an asymptote at a post stiffness of approximately $k = 100 \text{ nN}/\mu\text{m}$. Further increases in the post stiffness above this level do not affect the cell response.

4.2.2 Average Force Versus Post Stiffness

We calculate the average force per post F_{avg} as the sum of the magnitude of the force exerted by the cell on each post in contact with the cell divided by the number of posts. In Fig. 5 we plot F_{avg} versus post stiffness k for square cells having various edge lengths. To vary cell size, we utilize square cells of edge length $L = 10, 30$ and $50 \mu\text{m}$ laid on $3 \times 3, 8 \times 8$ and 14×14 post arrays, respectively. For each case, we vary the post stiffness from $k = 2 \text{ nN}/\mu\text{m}$ to $k = 500 \text{ nN}/\mu\text{m}$ and plot the resulting F_{avg} values in Fig. 5. In all cell sizes, we find a common trend between average

force and post stiffness; namely, the average force per post F_{avg} increases with post stiffness, but reaches an asymptote. We also find that this trend prevails even if the post-bed parameters, such as post diameter and post density, are varied, but do not present these results here. The relationship between average force and post stiffness observed in our simulations agrees qualitatively as well as quantitatively with the experimental results of Saez et al. (2005), presented as a superimposed line in Fig. 5. It is this quantitative agreement that is used to justify the parameter calibration used throughout the simulations presented in this paper.

We note that the results of our simulations for cells on posts confirm that the average force generated by the cell is higher on stiffer substrates, and reaches a limit value beyond a critical value of substrate stiffness. This trend is consistent with our findings in the simulations for cells adhered on flat substrates, as presented in the previous section (Fig. 2(b)).

Tan et al. (2003) observed in experiments that the average force per post for a given post stiffness increases with cell size, and therefore with the number of posts to which the cell is adhered. Simulations by Deshpande et al. (2007) found the same trend, and they attributed this feature to the fact that a cell contracting on many posts senses a stiffer system than one contracting on a few posts. Deshpande et al. (2007) pointed out that this trend occurs despite the fact that many of the posts under well-spread cells engaging many posts are only lightly laden, due to the fact that these posts are in the central region of the cell where the cell stress is relatively uniform (see Fig. 4(c)). To further explore the effect of cell size on cellular contractility, we study how the average force per post varies with cell edge length for four post stiffnesses, with results shown in Fig. 6. We note that the cells engage 3×3 , 4×4 , 6×6 , 8×8 , 11×11 and 14×14 posts as they get larger. For each cell size the average force per post increases with post stiffness. Furthermore, as the smallest cell size is increased, the trend, the same for all post stiffnesses, is that the average force per post increases. In the case of the cell on the most compliant posts, this trend is monotonic. However, in all other cases, a peak in the average force per post is reached at an intermediate cell size, beyond which the average force per post falls.

The trend in which the average force per post increases with cell size, also observed by Deshpande et al. (2007), reflects the fact that a cell engaging more posts is interacting with a stiffer system. Since a stiffer environment induces in the cell a more robust cytoskeleton, and a higher level of contractile stress, the force per post goes up as the cell size increases. The trend in which the force per post declines as the cell size increases reflects the fact that a cell engaging a larger number of posts has a larger number that are lightly laden because they are near the center of the cell in the region of uniform cell stress. Since an increasing number of posts has negligible force applied to them, the force per post goes down as the cell size increases. The results in Fig. 6 indicate that the former trend dominates for small cells engaging a small number of posts, but as the cell size increases, the latter trend takes over. The results in Fig. 6 also show that the transition point for these opposite trends depends on the stiffness of the posts. In a stiff environment, the changeover occurs at smaller cell size, whereas in a more compliant environment, a larger cell size is required for the transition.

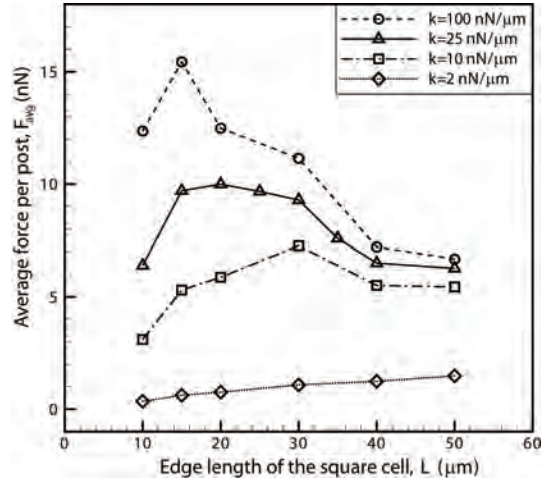


Fig. 6 Average force per post F_{avg} exerted by a square cell in steady state versus its edge length L plotted for post stiffness values $k = 2, 10, 25$ and 100 nN/ μm .

5 Concluding remarks

A bio-chemo-mechanical model is employed for modeling cell behavior in complex and diverse extra-cellular settings, and the effects of substrate stiffness, architecture of the substrate, and cell area are studied. Both on flat gel and micro-post substrates, cell contractility and focal adhesion assembly intensify as the stiffness of the environment is increased. The results of our simulations match key experimental data in the literature. We verify some well-established features regarding cell behavior in response to substrate stiffness—namely, (a) the intracellular force generation machinery exerts higher forces on stiffer substrates, (b) cells form larger and stronger focal adhesions on stiffer substrates, and (c) cells on stiffer substrates have more pronounced cytoskeletons in the form of higher concentrations of stress fibers. The response we have identified comes about because a stiff substrate presents resistance to the cell as it tries to contract, an effect that stabilizes a high degree of stress fiber polymerization and focal adhesion development. Such highly developed intracellular machinery then delivers a high level of traction to the substrate. We also find that monotonic increase of the stiffness of the substrate does not cause a monotonic enhancement of the cellular contractile machinery; an asymptote is reached at a critical value of substrate stiffness beyond which further enhancement of the cell contractile system ceases. Such a behavior is hinted at in the results from several experimental studies, such as that of Saez et al. (2005), but a conclusive dataset for a wide range of substrate stiffness values is currently unavailable. Our results not only agree qualitatively with many experimental findings, but have been calibrated quantitatively to the average force per post from Saez et al. (2005), where the stiffness of the posts is varied. This step enables us to assert that the cell model parameters used in our

study are representative of the epithelial cells explored by Saez et al. (2005). The horseshoe focal adhesions on the post tops that we obtain in our simulations match the experimental images obtained by Tan et al. (2003) and Chen et al. (2003). Such results give us encouragement to believe that our model captures many elements of the contractile and adhesive behavior of cells, and may prove useful, eventually, in a wider setting of cell biology, medicine and disease.

Acknowledgements AP, AGE and RMM were supported by a Multi-University Research Initiative sponsored by the U.S. Army Research Office. RMM was also supported by Aberdeen University and by INM-Leibniz Institute for New Materials. VSD acknowledges the support of the Isaac Newton Trust, Trinity College, Cambridge.

References

- Boudreau, N., Bissell, M. J., 1998. Extracellular matrix signaling: integration of form and function in normal and malignant cells. *Curr. Opin. Cell Biol.* 10, 640–646.
- Chen, C. S., Alonso, J. L., Ostuni, E., Whitesides, G. M., Ingber, D. E., 2003. Cell shape provides global control of focal adhesion assembly. *Biochem. Biophys. Res. Commun.* 307, 355–361.
- Deshpande, V. S., McMeeking, R. M., Evans, A. G., 2006. A bio-chemo-mechanical model for cell contractility. *Proc. Natl. Acad. Sci. USA* 103, 14015–14020.
- Deshpande, V. S., McMeeking, R. M., Evans, A. G., 2007. A model for the contractility of the cytoskeleton including the effects of stress fiber formation and dissociation. *Proc. R. Soc. Lond. A* 463, 787–815.
- Deshpande, V. S., Mrksich, M., McMeeking, R. M., Evans, A. G., 2008. A bio-mechanical model for coupling cell contractility with focal adhesion formation. *J. Mech. Phys. Solids* 56, 1484–1510.
- Discher, D. E., Janmey, P., Wang, Y.-L., 2005. Tissue cells feel and respond to the stiffness of their substrate. *Science* 310, 1139–1143.
- Gaskell, D. R., 1973. *Introduction to Metallurgical Thermodynamics*. New York, McGraw-Hill.
- Kong, H. J., Liu, J., Riddle, K., Matsumoto, T., Leach, K., Mooney, D. J., 2005. Non-viral gene delivery regulated by stiffness of cell adhesion substrates. *Nat. Mater.* 4, 460–464.
- Lennard-Jones, J. E., 1931. Cohesion. *Proc. Phys. Soc.* 43, 461–482.
- Lo, C.-M., Wang, H.-B., Dembo, M., Wang, Y., 2000. Cell movement is guided by the rigidity of the substrate. *Biophys. J.* 79, 144–152.
- McCleverty, C. J., Liddington, R. C., 2003. Engineered allosteric mutants of the integrin $\alpha M\beta 2$ I domain: structural and functional studies. *Biochem. J.* 372, 121–127.
- Paszek, M. J., Zahir, N., Johnson, K. R., Lakins, J. N., Rozenberg, G. I., Gefen, A., Reinhart-King, C. A., Margulies, S. S., Dembo, M., Boettiger, D., Hammer,

- D. A., Weaver, V. M., 2005. Tensional homeostasis and the malignant phenotype. *Cancer cell* 8, 241–254.
- Pathak, A., Deshpande, V. S., McMeeking, R. M., Evans, A. G., 2008. The simulation of stress fiber and focal adhesion development in cells on patterned substrates. *J. R. Soc. Interface* 5, 507–524.
- Pathak, A., McMeeking, R. M., Evans, A. G., Deshpande, V. S., 2011. An analysis of the cooperative mechano-sensitive feedback between intracellular signaling, focal adhesion development, and stress fiber contractility. *J. Appl. Mech.* 78, 041001.
- Saez, A., Buguin, A., Silberzan, P., Ladoux, B., 2005. Is the mechanical activity of epithelial cells controlled by deformations or forces? *Biophys. J.* 89, L52–L54.
- Schwartz, M. A., Ginsberg, M. H., 2002. Networks and crosstalk: integrin signaling spreads. *Nat. Cell Biol.* 4, E65–68.
- Shemesh, T., Geiger, B., Bershadsky, A. D., Kozlov, M. M., 2005. Focal adhesions as mechanosensors: a physical mechanism. *Proc. Natl. Acad. Sci. USA* 102, 12383–12388.
- Tan, J. L., Tien, J., Pirone, D. M., Gray, D. S., Bhadriraju, K., Chen, C. S., 2003. Cells lying on a bed of microneedles: An approach to isolate mechanical force. *Proc. Natl. Acad. Sci. USA* 100, 1484–1489.
- Wei, Z., Deshpande, V. S., McMeeking, R. M., Evans, A. G., 2008. Analysis and interpretation of stress fiber organization in cells subject to cyclic stretch. *J. Biomech. Eng.* 130, 031009.
- Yeung, T., Georges, P. C., Flanagan, L. A., Marg, B., Ortiz, M., Funaki, M., Zahir, N., Ming, W., Weaver, V., Janmey, P. A., 2005. Effects of substrate stiffness on cell morphology, cytoskeletal structure, and adhesion. *Cell Motil. Cytoskeleton* 60, 24–34.